Article

Molecular Cell

Autonomous Metabolic Oscillations Robustly Gate the Early and Late Cell Cycle

Graphical Abstract

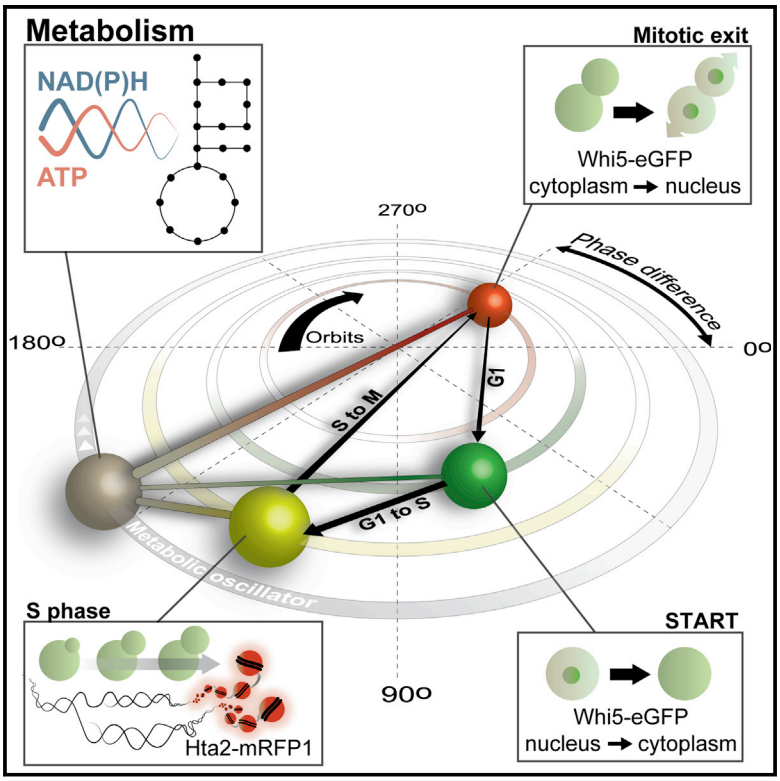

Highlights

- Metabolic cycles are an intrinsic, growth-condition-independent behavior of single cells
- The metabolic oscillations are not the result of the cell cycle and thus are autonomous
- The metabolic oscillator and the cyclin/CDK machinery form a system of coupled oscillators
- Both the early and late cell cycle operate in coordination with the metabolic oscillator

Authors

Alexandros Papagiannakis, Bastian Niebel, Ernst C. Wit, Matthias Heinemann

Correspondence

m.heinemann@rug.nl

In Brief

Papagiannakis et al. performed metabolite and cell-cycle measurements in single cells to show that the cell cycle is a higher-order function, which emerges from the collective synchrony between an autonomous metabolic oscillator, a biomass formation oscillator (early cell cycle), and a biomass segregation oscillator (late cell cycle).

Papagiannakis et al., 2017, Molecular Cell 65, 285–295
January 19, 2017
http://dx.doi.org/10.1016/j.molcel.2016.11.018

CellPress

Molecular Cell
Article

Autonomous Metabolic Oscillations Robustly Gate the Early and Late Cell Cycle

Alexandros Papagiannakis,[1] Bastian Niebel,[1] Ernst C. Wit,[2] and Matthias Heinemann[1,3,*]
[1]Molecular Systems Biology, Groningen Biomolecular Sciences and Biotechnology Institute, University of Groningen, Nijenborgh 4, 9747 AG Groningen, the Netherlands
[2]Probability and Statistics, Johann Bernoulli Institute of Mathematics and Computer Science, University of Groningen, Nijenborgh 9, 9747 AG Groningen, the Netherlands
[3]Lead Contact
*Correspondence: m.heinemann@rug.nl
http://dx.doi.org/10.1016/j.molcel.2016.11.018

SUMMARY

Eukaryotic cell division is known to be controlled by the cyclin/cyclin dependent kinase (CDK) machinery. However, eukaryotes have evolved prior to CDKs, and cells can divide in the absence of major cyclin/CDK components. We hypothesized that an autonomous metabolic oscillator provides dynamic triggers for cell-cycle initiation and progression. Using microfluidics, cell-cycle reporters, and single-cell metabolite measurements, we found that metabolism of budding yeast is a CDK-independent oscillator that oscillates across different growth conditions, both in synchrony with and also in the absence of the cell cycle. Using environmental perturbations and dynamic single-protein depletion experiments, we found that the metabolic oscillator and the cell cycle form a system of coupled oscillators, with the metabolic oscillator separately gating and maintaining synchrony with the early and late cell cycle. Establishing metabolism as a dynamic component within the cell-cycle network opens new avenues for cell-cycle research and therapeutic interventions for proliferative disorders.

INTRODUCTION

Initiation and progression of the cell cycle are considered to occur in response to the timely ordered transcriptional, post-transcriptional, and post-translational regulation of the cell cycle (cyclin/cyclin dependent kinase [CDK]) machinery components (Barik et al., 2010; Coudreuse and Nurse, 2010; Tyson and Novak, 2008). However, there is evidence that a cell-cycle regulator external to the cyclin/CDK machinery provides triggers for cell-cycle initiation or progression. First, cell-cycle entry can occur even in the absence of major cell-cycle machinery components (e.g., the early cyclins) (Sherr and Roberts, 2004). Second, late cell-cycle proteins (e.g., cdc14 and sic1) (Lu and Cross, 2010; Rahi et al., 2016), and possibly also global transcription (Haase and Reed, 1999; Orlando et al., 2008), continue to oscillate in cell-cycle-arrested cells. Third, the eukaryotic cell cycle evolved before CDKs, and thus, the early eukaryotes must have employed non-CDK cell-cycle regulators (Krylov et al., 2003).

Because metabolism oscillates in synchrony with (Brunetti et al., 2016; Futcher, 2006; Klevecz et al., 2004; Müller et al., 2003; Silverman et al., 2010; Tu et al., 2005, 2007; Xu and Tsurugi, 2006) and, as suggested, without the cell cycle (Novak et al., 1988; Slavov et al., 2011), and because metabolic checkpoints exist in the cell-cycle program (Jones et al., 2005; Saqcena et al., 2013; Takubo et al., 2013), we conjectured that metabolism operates as an autonomous, cell-cycle-independent oscillator, which together with the cell cycle might form a system of coupled oscillators. In response to nutrients, the metabolic oscillator could orbit with different frequencies and provide periodic triggers for cell-cycle initiation and progression. Interactions between metabolites and cell-cycle proteins (Buchakjian and Kornbluth, 2010; Lee and Finkel, 2013; Shi and Tu, 2013; Yalcin et al., 2014) could convey those triggers, and in reverse, the cell cycle could entrain metabolism via the regulation of enzyme activity (Ewald et al., 2016; Lee et al., 2014; Tudzarova et al., 2011; Wang et al., 2014; Zhao et al., 2016).

Here, using methods for the dynamic quantification of metabolites in single cells, in combination with microfluidics and time-lapse microscopy, we demonstrate that the metabolism of budding yeast is an oscillator, which orbits autonomously of the cell cycle. Perturbation experiments, including dynamic nutrient shifts as well as conditional and targeted depletion of cell-cycle proteins, revealed that the metabolic oscillator, together with the cell cycle, forms a system of coupled oscillators. The metabolic and the cell-cycle oscillators accomplish frequency synchrony—required for the activation and progression of the cell-division program—only within a certain window of metabolic frequencies, whereas the robust gating of the cell-cycle phases by metabolic dynamics ensures the temporal separation of biomass production (early cell cycle) and segregation (late cell cycle). Our findings demonstrate that the metabolic oscillator is an indispensable component of cell-cycle regulation, open new research avenues into cell-cycle control, and suggest the metabolic oscillator as a global therapeutic target against proliferative disorders.

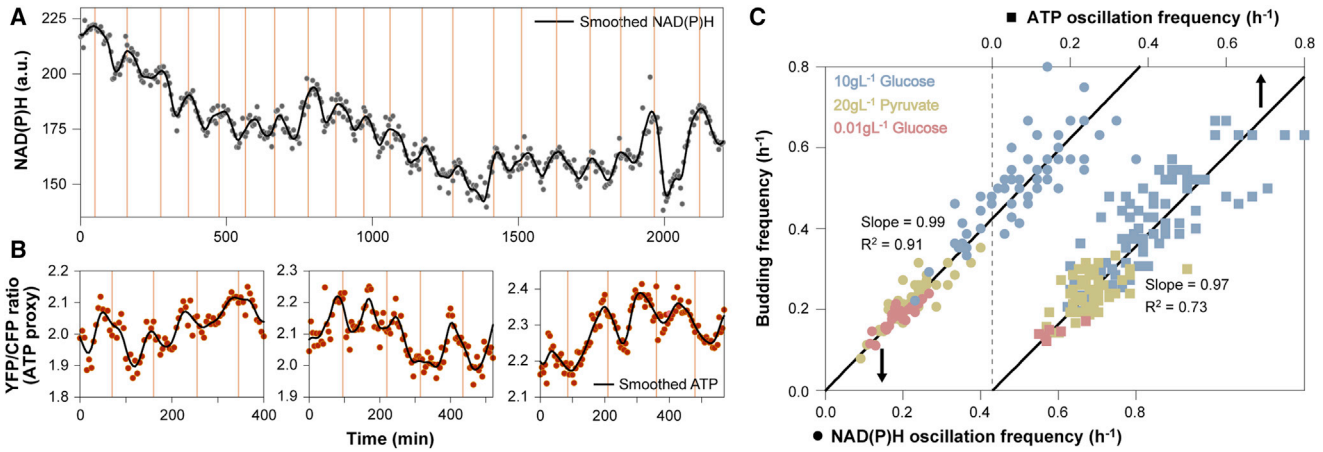

Figure 1. Metabolism Oscillates in Single Cells, across Nutrients, and in Frequency Synchrony with the Cell Cycle

(A) Oscillating NAD(P)H levels in a single cell.

(B) Oscillating ATP levels (three single cells) dynamically measured using the ATeam 1.03 FRET sensor (Imamura et al., 2009) (see also Figures S1A, S1B, and S1D–S1H). Cells were grown on high glucose (10 gL^{-1}), in the absence of synchronization (Figure S1C). Black lines indicate smoothing splines used for visualization. Vertical orange lines indicate budding.

(C) Budding and the frequency of NAD(P)H and ATP oscillations correlate across growth conditions; n = 38 cells with 137 NAD(P)H oscillations (solid circles) and 38 cells with 136 ATP oscillations (solid squares). Time periods between consecutive buddings, or consecutive peaks of NAD(P)H and ATP oscillations, were used to determine budding and oscillation frequency data, respectively. Linear regressions (black diagonals) illustrate the correlations. The greater noise in the ATP oscillation frequency estimation (Figures S2A and S2B) is reflected in the different R^2 values for NAD(P)H and ATP.

RESULTS

Metabolic Cycles Are an Intrinsic, Growth-Condition-Independent Behavior of Single Cells

To test our hypothesis, after which metabolism is an oscillator that is coupled to the cell cycle, we used *Saccharomyces cerevisiae* as a model. First, we asked whether a metabolic oscillator exists. Because it has been conjectured that population-level cell-cycle synchronization and cell-to-cell communication artificially induce metabolic oscillations (Aon et al., 2007; Laxman et al., 2010; Sohn et al., 2000), we investigated metabolic and cell-cycle dynamics on the single-cell level. We used a microfluidic device for the long-term microscopic observation of single budding yeast cells (Huberts et al., 2013), the auto-fluorescence of the reduced nicotinamide nucleotide NAD(P)H, to assess its intracellular levels (Gustavsson et al., 2012; Lloyd et al., 2002), and a protein-based Förster resonance energy transfer (FRET) sensor to measure ATP (Imamura et al., 2009). Optimization of the sensor expression and imaging settings led to adequate signal intensities with marginal cellular photo-damage and photo-toxicity during long-term (>12 hr) imaging (Figures S1A and S1B).

Using these tools, we first investigated whether periodic NAD(P)H and ATP fluctuations occur in single cells, grown on high (10 gL^{-1}) glucose without cell-to-cell communication or cell-cycle synchronization (Figure S1C). These fluctuations, subsequently identified (Figures 1A and 1B; Movie S1) and confirmed by autocorrelation analysis (Figures S2A and S2B), occurred with an average period of ~2 hr, which corresponds to the average doubling time under this condition. Through comparative analyses, we validated that the measured single-cell FRET signals reflect intracellular ATP concentrations (Figures S1D–S1H). Because the ATP and NAD(P)H signals oscillate oppositely in phase (Figures S2C and S2D), we conclude that the measured metabolite dynamics are not due to a correlated variability (such as periodic volume chances). Given the absence of cell-cycle synchronization (Figure S1C), our findings demonstrate that, contrary to previous reports (Aon et al., 2007; Laxman et al., 2010; Sohn et al., 2000), metabolic cycles with periods in the hour range are an intrinsic behavior of single cells.

To test whether metabolic cycles also occur in other growth conditions, we subjected yeast to different nutrients and metabolic operations (aerobic fermentation, respiration, and gluconeogenesis), which varied the doubling time in single cells from 1.4 to 11 hr. Despite these different metabolic operations, we consistently identified oscillations in the NAD(P)H and ATP levels (Figures S2E–S2J), demonstrating that the metabolic cycles occur regardless of growth conditions.

To investigate whether the metabolic cycles occur in synchrony with the cell cycle, we correlated the frequencies of budding with the frequencies of the NAD(P)H or ATP oscillations. Despite the wide range of doubling times across nutrient conditions, the budding frequencies always matched the frequencies of the corresponding NAD(P)H or ATP oscillations (Figure 1C). Thus, the metabolic oscillations and the cell cycle operate in frequency synchrony over the range of growth conditions tested, which suggests a coupling between the two periodic processes.

The Metabolic Oscillations Are Not the Result of the Cell Cycle and Thus Are Autonomous

To determine if the metabolic oscillations are a mere consequence of cell-cycle operation or if they occur in a cell-cycle-independent manner and thus are autonomous, we searched

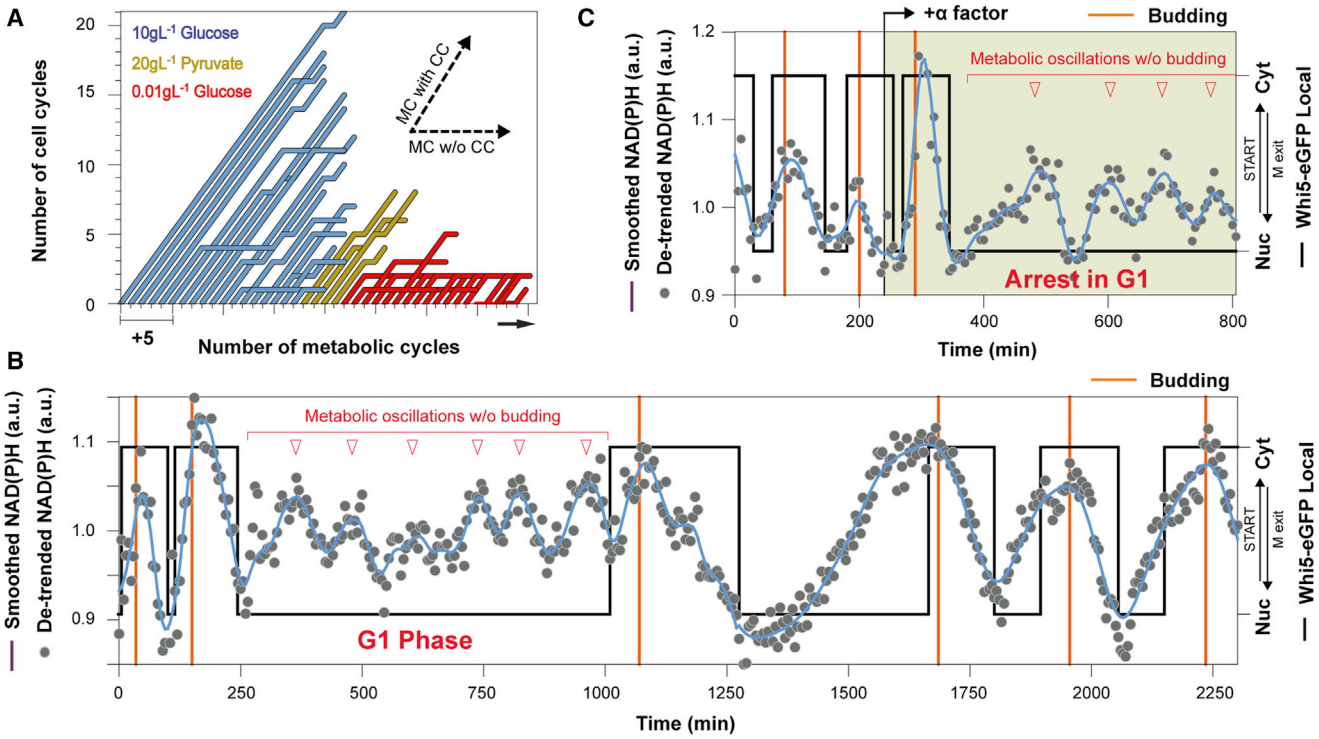

Figure 2. Metabolic Oscillations Are Independent of the Cell Cycle

(A) Metabolic oscillations without cell-cycle initiation occur spontaneously under all growth conditions (see also Figures S3A and S3B). Each line corresponds to a single cell. Diagonal trajectories indicate metabolic cycles (MC) in synchrony with budding and the cell cycle (CC); horizontal trajectories show "uncoupled" MCs without budding.

(B) After two coupled MC/CC events, spontaneous G1 arrest occurred at 245 min in a single cell (grown on 10 gL^{-1} glucose), and the metabolic oscillations continued (see also Movie S2). Arrest persisted for 765 min, before resumption of MC/CC synchrony. NAD(P)H oscillations are indicated by gray lines, Whi5-eGFP localization by black lines (see also Figures S4A and S4C) and the budding events by orange lines (see also Figure S4B). Red triangles indicate peaks of metabolic oscillations without budding.

(C) Mating pheromone alpha factor (added at 240 min) caused cell-cycle arrest in G1 and the metabolic oscillations continued (data for a single cell grown on 10 gL^{-1} glucose) (see also Figure S5).

in our single-cell data for metabolic oscillations that were unaccompanied by cell-cycle progression. Such events occurred for all growth conditions (Figures 2A, S3A, and S3B), with an approximate incidence of 1/50 metabolic oscillations on 10 gL^{-1} glucose. On 0.01 gL^{-1} glucose, we also found many cells with consecutive metabolic oscillations without cell-cycle progression (Figures 2A, S3C, and S3D).

To determine the cell-cycle status of the non-dividing cells, we used a strain with fluorescently tagged Whi5, a transcriptional repressor of early cyclins and target of CDK phosphorylation. Whi5 sequesters into the nucleus at late mitosis (hereafter denoted as "M exit") and exits upon phosphorylation at late G1 (denoted as "START"), reporting an active CDK (Bloom and Cross, 2007; Costanzo et al., 2004; Ferrezuelo et al., 2012) (Figures S4A–S4C). Using this reporter, we found that cells with metabolic oscillations but without an accompanying cell cycle were either arrested at G1 (i.e., Whi5 in the nucleus; Figure 2B; Movie S2) or occasionally after budding in a non-G1 phase (i.e., Whi5 in the cytoplasm; Movie S3).

To substantiate the finding that metabolic oscillations are not the consequence of the cell-cycle operation, we added the mating pheromone (alpha factor), which induces G1 arrest (Bardwell, 2004), to cells growing in the microfluidic device. Also after the pheromone-induced cell-cycle arrest, the NAD(P)H levels continued to oscillate (Figures 2C and S5). Together, these findings demonstrate that the metabolic oscillations are not the result of cell-cycle operation and CDK activity but constitute an autonomous behavior of metabolism, occurring across growth conditions. The autonomy of the metabolic oscillator, and its frequency synchrony with the cell cycle (Figure 1C) in normally dividing cells, suggest metabolism as a separate component in the cell-cycle control engine.

The Metabolic Oscillator and the Cell Cycle Form a System of Coupled Oscillators

We conjectured that the metabolic oscillator and the cell-cycle oscillator form a system of coupled oscillators, similar to other instances of synchrony in biology, including the rhythmic flashes of fireflies or the synchronized discharge of cardiac pacemaker cells (Strogatz, 2001). Analogously to the fact that an effective contraction of the heart muscle requires a strict synchrony between cells in the sinoatrial node, cell-cycle control could emerge from the coupling and mutual entrainment between the metabolic oscillator and the cell-cycle oscillator.

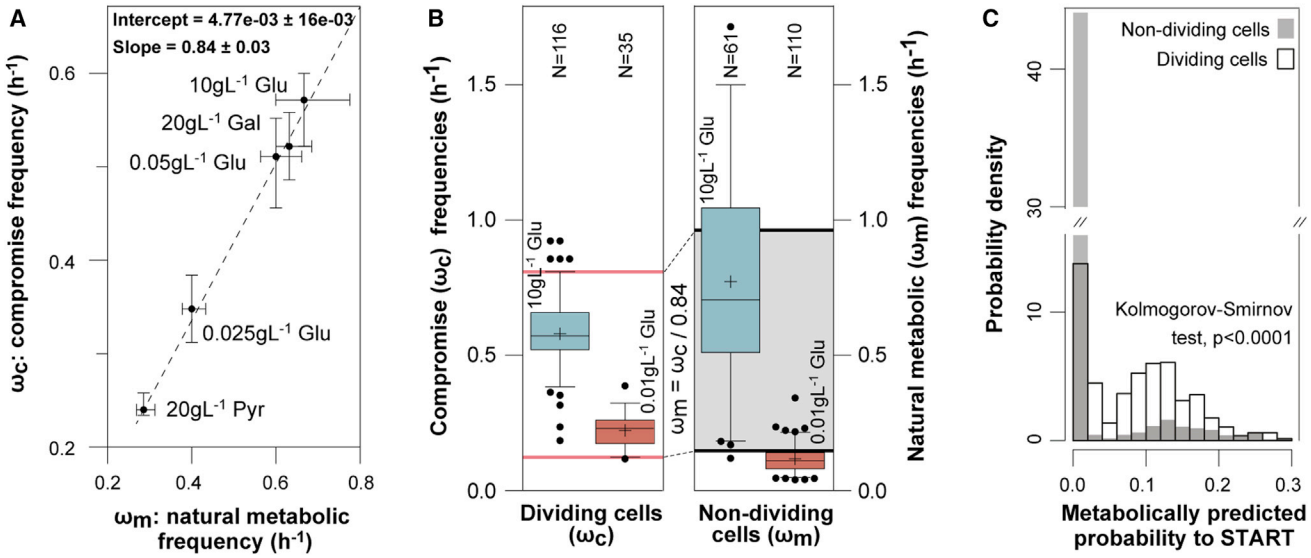

Figure 3. Coupling Slows Down the Metabolic Oscillator and Occurs Only within a Window of Natural Metabolic Frequencies

(A) Median compromise frequencies measured in dividing cells versus median natural metabolic frequencies measured in alpha-factor-arrested cells (as in Figure S5) under different growth conditions. Both frequencies were estimated from consecutive trough intervals in single-cell NAD(P)H oscillations. Median frequencies and their 95% confidence intervals (error bars) were estimated using non-parametric bootstrapping. The slope and intercept of the fitted line with SEs are indicated.

(B) The frequencies of metabolic oscillations with or without cell cycle, measured during growth on high (10 gL^{-1}) and low (0.01 gL^{-1}) glucose (error bars: 5–95 percentiles). Natural metabolic frequencies were measured in cells spontaneously skipping one or more cell cycles (e.g., Figures 2B, S3A, and S3C). Crosses indicate distribution means. Natural metabolic frequencies necessary for cell cycle initiation (gray shaded area) were estimated by dividing the fastest (95th percentile, 10 gL^{-1} glucose) and slowest compromise frequencies (fifth percentile, 0.01 gL^{-1} glucose) by 0.84 (estimated slope in Figure 3A).

(C) The probabilities for cell-cycle START based on the dynamics of the NAD(P)H signal are significantly different for dividing (white bars) versus non-dividing cells (gray bars) on low glucose. Probabilities were computed using predictive densities based on a Cox proportional hazards analysis (Cox, 1972) and reflect the hazard of a START event with NAD(P)H dynamics as a time-dependent covariate (hazard function analysis – Supplemental Experimental Procedures). The accuracy of prediction is ~70% (receiver-operating characteristic [ROC] analysis).

To investigate whether the metabolic oscillator and the cell cycle indeed form a coupled oscillator system, we searched for signature features of such systems by means of steady-state and dynamic perturbations. A common characteristic of coupled oscillators is that their natural frequencies (i.e., the frequency of each individual oscillator when uncoupled) converge to a common compromise frequency (i.e., the common frequency of the oscillators when they are coupled) proportional to the strength of their coupling (Strogatz, 2014). We determined the frequency of the metabolic oscillator in the presence of cell cycle (compromise frequency) in normally dividing cells and in the absence of cell-cycle progression (natural frequency of the metabolic oscillator), the latter in cells where the cell cycle was arrested with the alpha factor (Figure S5). In line with the theory of coupled oscillators (Strogatz, 2014), we found a linear correlation between the natural metabolic and compromise frequencies under different conditions (Figure 3A). The compromise frequency was routinely 16% lower than its corresponding natural metabolic frequency (Figure 3A), a reduction that could be interpreted as a load imposed on the metabolic oscillator by the cell cycle upon coupling.

Another distinctive feature of coupled oscillator systems is that coupling and synchrony are only accomplished when the natural frequencies of the individual oscillators are proximal (Nolte, 2015; Strogatz, 2014). With different nutrient conditions resulting in different natural frequencies for the metabolic oscillator (Figure 3A), we investigated at which natural metabolic frequencies coupling with the cell cycle occurs. Here, we found that at very low metabolic frequencies and at very high ones, no coupling occurred (Figure 3B). Given the standardized reduction of the compromise frequency (16%) (Figure 3A), we identified the range of natural metabolic frequencies from 0.15 h^{-1} to 0.96 h^{-1} to enable coupling (Figure 3B). On 0.01 gL^{-1} glucose, 75% of the metabolic oscillations without cell cycle (Figures S3C and S3D) had a natural metabolic frequency below the estimated threshold for coupling and thus cell-cycle initiation (Figure 3B), resulting in a substantial fraction of non-dividing cells. A statistical analysis (hazard function analysis; Supplemental Experimental Procedures) of the dynamic NAD(P)H signals and START occurrence further demonstrates the importance of the metabolic frequency for coupling and cell-cycle initiation (Figure 3C). These findings reveal a second characteristic of coupled oscillators: coupling between the metabolic oscillator and the cell cycle is only achieved within a window of natural metabolic frequencies; lower or higher metabolic frequencies are not sufficient for coupling and thus for cell-cycle initiation.

Another characteristic of coupled oscillators is phase gating, i.e., the maintenance of a relative phase between oscillators in synchrony (Feillet et al., 2014; Mori et al., 1996). Initially focusing on cells grown on high (10 gL^{-1}) glucose, we found strict phase

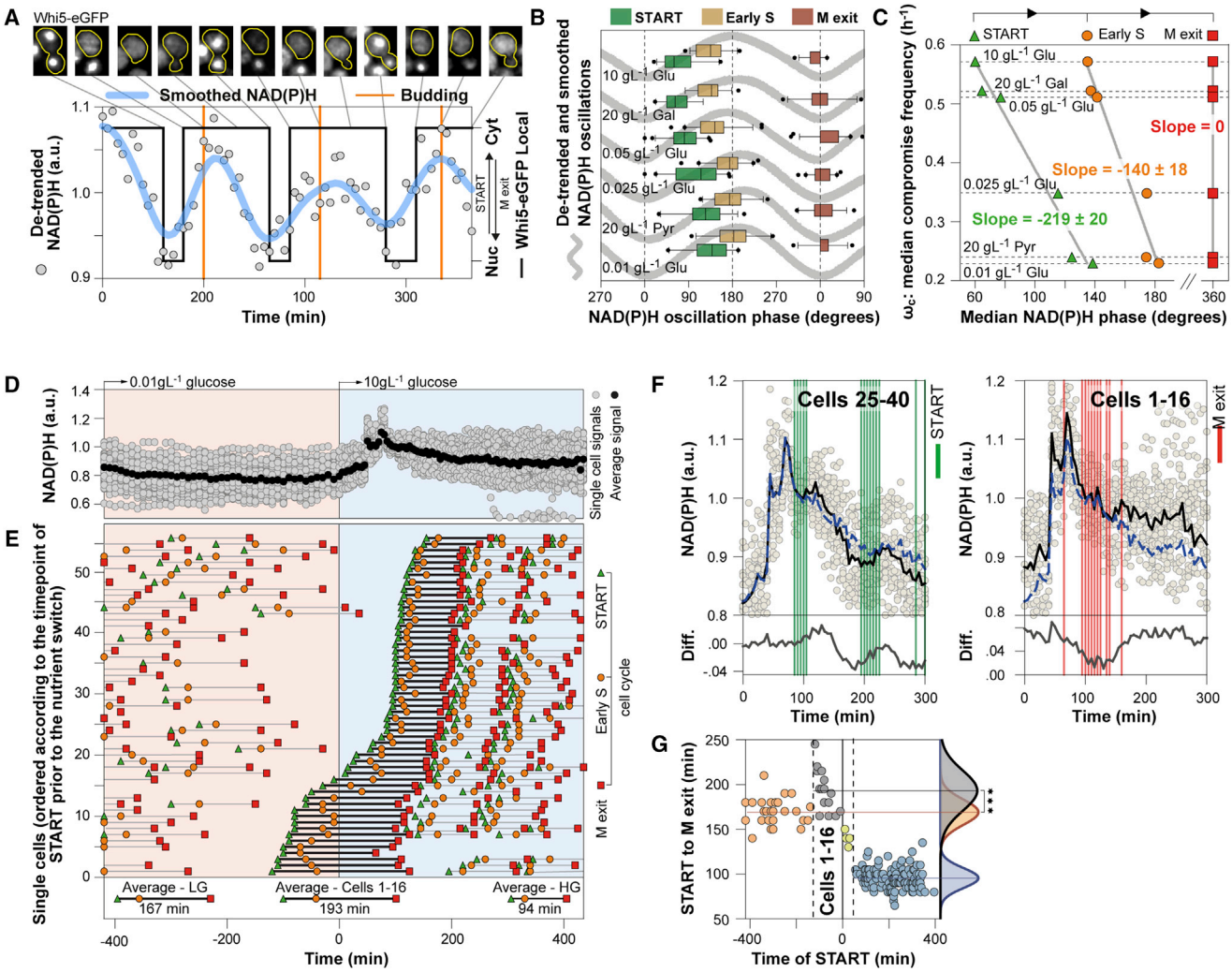

Figure 4. Cell-Cycle Events Are Robustly Gated to Distinct Metabolic Phases

(A) Whi5-eGFP translocations (cytosolic [cyt] and nuclear [nuc]; black lines), together with the NAD(P)H signals in a single cell growing on high glucose. Orange lines denote budding.

(B) The distributions of START, budding, and M exit on the NAD(P)H oscillations at different growth conditions; error bars represent fifth to 95th percentiles (10 gL^{-1} glucose, 31 oscillations from five single cells; 20 gL^{-1} glucose, 31 oscillations from eight cells; 0.05 gL^{-1} glucose, 46 oscillations from 16 cells; 0.025 gL^{-1} glucose, 44 oscillations from four cells; 20 gL^{-1} pyruvate, 27 oscillations from 26 cells; 0.01 gL^{-1} glucose, 20 oscillations from 13 cells).

(C) Median NAD(P)H phase at START, budding, and M exit with median compromise frequencies under different nutrient conditions.

(D) Metabolic response to glucose upshift (from 0.01 gL^{-1} to 10 gL^{-1}) at 0 min. NAD(P)H signals from 56 cells normalized to the 100-min signal.

(E) Timing of START (triangle), budding (circle), and M exit (square) for 56 cells ordered by the START time closest to the nutrient switch. The average cell-cycle durations according to glucose concentration (low glucose [LG], 0.01 gL^{-1}; high glucose [HG], 10 gL^{-1}) and when interrupted by the nutrient switch (cells 1–16) are indicated.

(F) START (green lines) is confined to the ascending part of the NAD(P)H oscillation following the metabolic response (cells 25–40); M exit (red lines) is restricted to the trough (cells 1–16). Single-cell (gray symbols) and averaged (black line) NAD(P)H signals are shown. The average NAD(P)H signal of the whole population (blue dashed line) was subtracted from subgroup (cells 25–40 or cells 1–16) averages (black line) to reveal the subgroup-specific NAD(P)H dynamics (labeled as "Diff.").

(G) The single-cell timing of START relative to its cell-cycle length (START to M exit), demonstrating the significant prolongation (***p value < 0.001, two-tailed t test, Shapiro-Wilk normality test, with Welch's correction for unequal variances) of the cell cycle as a result of the M exit confinement to the trough of the metabolic response. Normal distributions were fitted to data for low (red) and high (blue) glucose and for cells that were interrupted by the nutrient switch (gray).

gating of the cell-cycle events at specific metabolic phases: START and budding (i.e., early S phase; Figures S4D–S4F) consistently occurred at the ascending part of the oscillating NAD(P)H signal. Mitotic exit always occurred at the signal trough (Figures 4A, 2B, and 2C). ATP oscillations were shifted by ~180° (Figures S2C and S2D), with budding occurring at the descending part of the ATP signals (Figures S1E–S1H).

Next, we examined whether this pattern of phase gating is maintained under other nutrient conditions. We found that at decreased compromise frequencies, START and the early

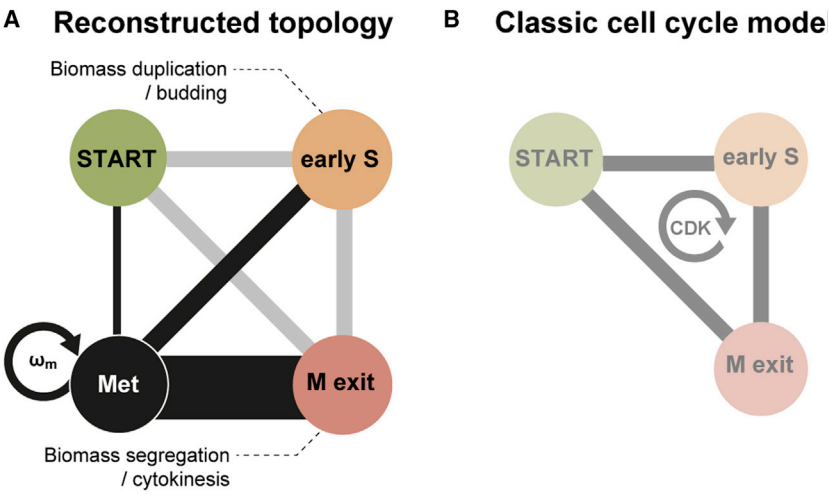

Figure 5. Interaction Topology between the Metabolic Oscillator and the Cell-Cycle Elements

(A) The reconstructed topology of cell cycle regulation. The black lines indicate couplings between the metabolic oscillator (MET) and the cell-cycle elements (START, early S phase, and M exit), scaled to their phase difference (Figure 4C). The gray lines indicate the classical connections between the cell-cycle phases. ω_m denotes the frequency of the metabolic oscillator. This model extends the classic, CDK-centric view (B) of cell-cycle regulation.

S phase shifted to later NAD(P)H phases (Figures 4B and 4C). In contrast, M exit always occurred at the troughs of the NAD(P)H oscillations, thus exhibiting a strict, condition-independent phase synchrony with metabolism (Figures 4B and 4C). The condition-independent gating of the late cell cycle (M exit) indicates its strong coupling to the metabolic oscillator. Adversely, the frequency-dependent phase gating of the early cell-cycle elements (START/early S) indicates a weaker coupling.

Next, to test the robustness of the phase gating, we dynamically perturbed metabolism by switching cells from low (0.01 gL^{-1}) to high (10 gL^{-1}) glucose and recorded their cell-cycle events. Upon the nutrient upshift, all cells responded with a strong, synchronously occurring peak in the NAD(P)H levels (Figure 4D), independently of their stage in the cell cycle (Figure 4E). Thereafter, the NAD(P)H oscillations continued with periods (START to M exit) matching those on high glucose (Figure 4E). Remarkably, those cells that had completed M exit before the nutrient shift (Figure 4E, cells 25–40), consistent with the phase gating under steady-state conditions (Figure 4B), would START only at the ascending part of the NAD(P)H oscillation following the metabolic response (Figure 4F, left), regardless of the timing of their prior M exit (Figure 4E, cells 25–40). Cells interrupted by the nutrient switch after START (Figure 4E, cells 1–16) showed significantly longer (two-tailed t test, p value < 0.001) cell-cycle duration, even when compared to those cultured on low glucose (Figure 4G, gray versus red symbols). Consistent with the observed steady-state and frequency-independent phase gating of M exit (Figure 4C), cells would only exit mitosis at the trough of their NAD(P)H oscillation following the metabolic response (Figure 4F, right), which prolonged their cell cycle (Figure 4G). Our results show that the gating of the cell-cycle phases by the metabolic oscillator is also maintained during dynamic metabolic perturbations and thus is robust. As a result, cell-cycle events are delayed even during nutrient upshifts, waiting for the "right" metabolic phase to occur after the metabolic perturbation, in order to maintain synchrony with the metabolic oscillator.

Together, the proportionality among the natural metabolic and compromise frequencies, the critical bandwidth of natural metabolic frequencies required for coupling and cell-cycle initiation, and the phase gating of the cell-cycle phases on the metabolic oscillator indicate that the metabolic oscillator and the cell-cycle oscillator form a system of coupled oscillators. Further, the autonomous nature of the metabolic oscillator, the robust phase gating of the cell-cycle events even during dynamic metabolic perturbations, and the dependency of cell-cycle initiation on the metabolic frequency suggest that the oscillating metabolism is an indispensable component in the cell-cycle regulation machinery, determining the timing of the cell-cycle phases and setting the pace of cell division.

The Early and Late Cell Cycle Are Separately Coupled to and in Coordination with the Metabolic Oscillator

On the basis of our data, we derived an interaction topology for the system of coupled oscillators, where the metabolic oscillator is coupled to and gates the phase of the early cell cycle (biomass duplication) and the late cell cycle (biomass segregation) (Figure 5A), operating in addition to the classic CDK-centric connections (Figure 5B). Because we observed the phase gating of M exit to be condition independent (Figure 4C) and to be maintained even during dynamic perturbations (Figure 4F, right), we postulate that a strong connection exists between the autonomous metabolic oscillator and the late cell cycle. If indeed strongly connected to the metabolic oscillator, the late cell cycle should also oscillate when the early cell cycle is halted. This notion is supported by the observations of Lu and Cross, who found periodic nucleolar or cytoplasmic localization of the Cdc14 phosphatase (an essential activator of the anaphase promoting complex and mitotic exit) in metaphase-arrested cells (i.e., in cells with fixed cyclin/CDK activity accomplished through stable non-degradable Clb2kd) (Lu and Cross, 2010). These findings demonstrate that the late cell cycle can oscillate even in the absence of early cell-cycle oscillations, supporting its strong coupling to the autonomous metabolic oscillator.

Further, according to the inferred interaction topology between the metabolic oscillator and the cell-cycle elements (Figure 5A), the metabolic oscillator should also be connected to the early cell cycle. If this is indeed true, the early cell cycle should continue to oscillate when the late cell cycle is halted. To test this, we halted the late cell cycle by dynamic depletion of Cdc14 using the yeast-adapted auxin-based degron system (Morawska and Ulrich, 2013; Nishimura et al.,

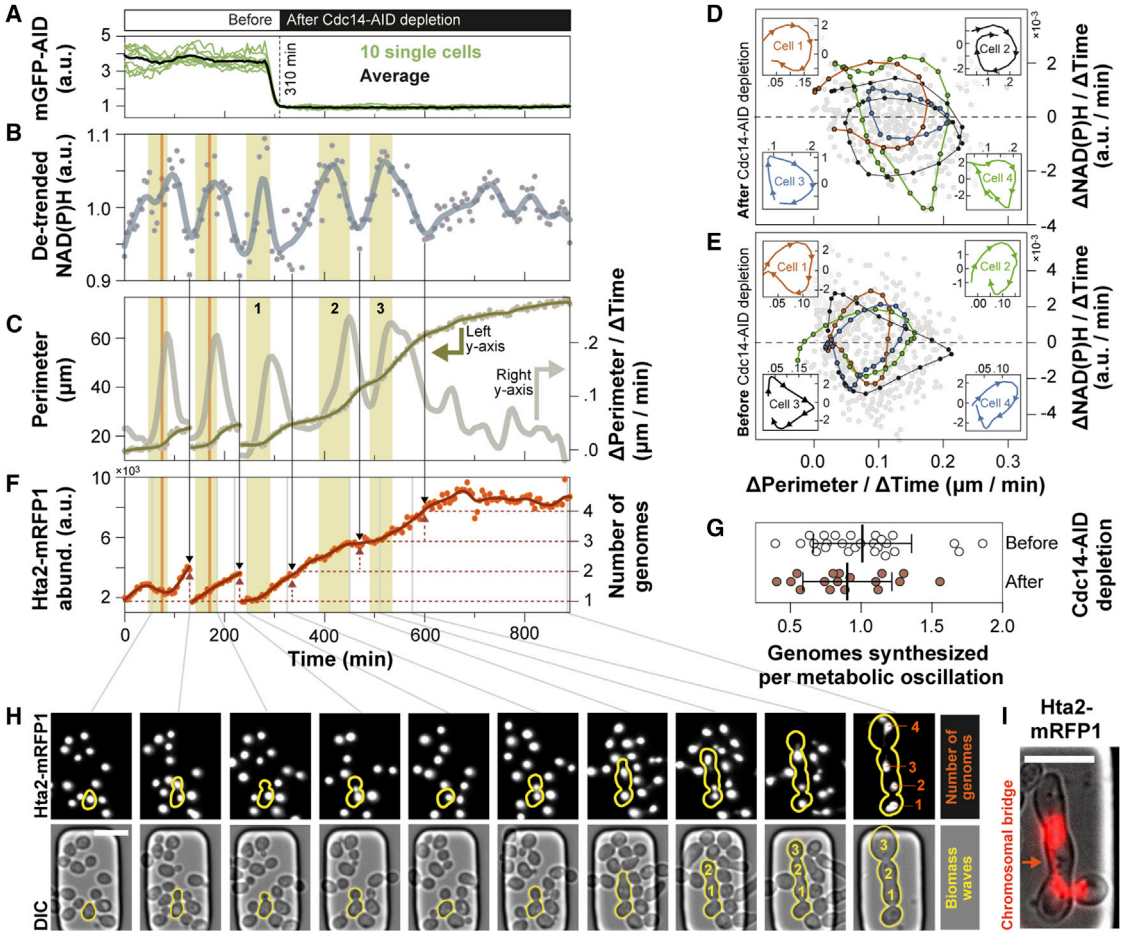

Figure 6. The Metabolic Oscillator Is Directly Coupled to the Early Cell Cycle

In this experiment, we arrested the late cell cycle (M exit) by dynamic depletion of Cdc14-AID at 310 min.

(A) mGFP-AID-expressing cells, present in the same microfluidic chip, were used to determine the timing of Cdc14-AID depletion upon the addition of auxin.

(B) Single-cell NAD(P)H levels continued to oscillate after the depletion of Cdc14 (gray line, smoothing spline for visualization).

(C) The rate of perimeter increase (right y axis), estimated from the smoothed cell perimeter (left y axis), used as a proxy of the biomass synthesis rate. Yellow areas indicate periods with rapid biomass synthesis where budding (vertical orange lines for first two cycles) occurs or would occur (in the cycles after Cdc14 depletion) (see also Movie S4). Three consecutive biomass synthesis waves occur after the last cytokinesis (last bud release before Cdc14 depletion) at 235 min, each in synchrony with the oscillating metabolism (cf. Figure 6B).

(D and E) The oscillating NAD(P)H and perimeter increase rates are coordinated in (D) late-cell-cycle-arrested cells similarly to (E) dividing cells (see also Figure S6). The respective single-cell signals are plotted against each other for each time point (gray markers). Exemplary trajectories from four single cells are presented for each condition (colored lines and markers).

(F) The histone Hta2-mRFP1 abundance, a reporter for the DNA content, was measured in the same cell (as in Figures 6B and 6C) prior and after the late cell-cycle arrest. During every metabolic oscillation (from trough to trough of the NAD(P)H signal), the DNA content (Hta2-mRFP1 abundance, left y axis) increased by the same amount before and also after Cdc14 depletion. The number of genomes (right y axis) were determined by dividing the Hta2 abundance at any given time point by the value at 240 min (just after cytokinesis), when cells have exactly one copy of their genome. Vertical black arrows extending from Figure 6B mark the troughs of each metabolic oscillation.

(G) Per metabolic oscillation, the Hta2-mRFP1 abundance increases by an amount corresponding to approximately one genome in dividing cells (before Cdc14-depletion, 26 oscillations from 15 single cells) and in Cdc14-depleted cells (17 oscillations from 11 single cells). Data from the metabolic oscillations, which were interrupted by the Cdc14-AID depletion (at 310 min), were not included in the analysis. Means and SD are presented. Both distributions passed the Shapiro-Wilk normality test.

(H) Microscopy images for certain time points (as indicated by gray lines) in the Hta2-mRFP1 and DIC channels show the increase in the DNA content and cell volume in the same single cell as in Figures 6B, 6C, and 6F (scale bar, 10 µm). After Cdc14 depletion, in the absence of cytokinesis, each of the three consecutive metabolic oscillations occurs in synchrony with one biomass production cycle (yellow numbers) and one DNA replication cycle.

(I) Chromosomal bridges, found in Cdc14-depleted cells using 100× magnification, confirm the late cell-cycle arrest (scale bar, 10 µm).

2009), an orthogonal system for the conditional and targeted protein degradation. First, following the dynamics of NAD(P)H, we found that the metabolic oscillations persisted after the arrest of the late cell cycle (Figures 6A and 6B; Movie S4), which was confirmed by the absence of cytokinesis (Figure 6C; Movie S4), also here witnessing the cell-cycle-autonomous nature of

the metabolic oscillator. Second, analyzing the dynamics of the cell size, we found that during the late cell-cycle arrest, biomass synthesis continued to occur in waves. Each wave was accompanied by one metabolic oscillation (Figures 6B and 6C; Movie S4). The clockwise phase correlation between oscillating NAD(P)H rates and oscillating cell volume increase rates in Cdc14-depleted cells (Figures 6D and S6) and dividing cells (Figures 6E and S6), confirms the coordination between the metabolic oscillator and early S also during late cell-cycle arrest. Remarkably, biomass synthesis waves ceased once the metabolic cycling stopped or its amplitude was low (Figures 6B and 6C).

To substantiate the connection between the metabolic oscillator and the early cell cycle, we tested whether DNA replication, an S phase reporter, also persists in Cdc14-depleted cells. As a dynamic single-cell measure of DNA replication, we used the histone H2A, tagged with mRFP1, previously (Rattray and Müller, 2012) and here (Figures 6F and 6G) shown to correlate with the DNA content. After the auxin-induced Cdc14 depletion and late cell-cycle arrest, we found that the amount of DNA continued to increase (Figures 6F–6H). The identified chromosomal bridges (Figure 6I), indicating spindle defects, absence of chromosomal abscission, and nuclear division (Amaral et al., 2016), additionally confirm late cell-cycle arrest. Each metabolic oscillation, also during late cell-cycle arrest, resulted in one additional genome (Figures 6G and 6H). Together, the sustained metabolic oscillations in the absence of late cell-cycle activity and the maintenance of their synchrony with cell size (biomass synthesis) and DNA content dynamics support a direct coupling of the metabolic oscillator to the early cell cycle.

DISCUSSION

Through dynamic monitoring of NAD(P)H and ATP levels as well as cell-cycle events in single cells, we found that metabolism is a cell-cycle-independent, nutrient-responsive oscillator, which together with the cell cycle forms a system of coupled oscillators. By means of steady-state and dynamic perturbations, we revealed that the metabolic oscillator is separately coupled to the early and late cell cycle, globally orchestrating biomass formation and segregation. Our findings demonstrate the biological significance of the metabolic oscillator. The cells are unable to progress through the cell cycle in the absence of an oscillating metabolism, and the oscillating metabolism dynamically gates the occurrence of the cell-cycle events (e.g., START and M exit) in response to nutrient changes.

The idea of endogenous oscillations in respiration or global protein synthesis setting the pace of the cell cycle was already suggested in the 1980s (Klevecz, 1969; Klevecz and Ruddle, 1968; Lloyd et al., 1982; Novak and Mitchison, 1987; Novak et al., 1988) but was abandoned soon after the discovery of the cyclin/CDK machinery (Watts, 2001), likely because the respective analyses of synchronized cultures did not generate broadly convincing data. Here, by exploiting the latest advances in single-cell technology (Huberts et al., 2013) and single-cell metabolite measurements to circumvent cell-cycle synchronization, in combination with targeted protein depletion (Morawska and Ulrich, 2013; Nishimura et al., 2009) to replace the classic temperature-sensitive mutants (Hartwell et al., 1974), we could demonstrate that metabolism is an autonomous oscillator, which together with the cell cycle forms a system of coupled oscillators. With these tools, we not only avoided potential synchronization (Aon et al., 2007; Laxman et al., 2010; Sohn et al., 2000) or temperature-related (Murray et al., 2001) artifacts but also used the inherent cell-to-cell variability to unravel the interactions between metabolism and the cell cycle.

Accordingly, cell-cycle control is not just the result of the cyclin/CDK machinery; it emerges from the collective synchrony between coupled and mutually entrained oscillators. While it has been suggested that the CDK oscillator locks the phase of ''peripheral oscillators,'' namely, Cdc14-release, the global transcription and centrosome duplication oscillators (Cross et al., 1989; Oikonomou and Cross, 2010), our work establishes the metabolic oscillator as an additional, key component within the cell-cycle control network. The metabolic oscillator and the cyclin/CDK machinery independently are not sufficient for cells to divide. Only the ensemble of the metabolic oscillator and cell-cycle oscillators (and eventually also the cell-cycle transcription program; Banyai et al., 2016; Hillenbrand et al., 2016; Rahi et al., 2016) exerts the higher-order function of cell-cycle control. Thus, our discovery does not undermine the importance of the cyclin/CDK machinery but expands the current view of cell-cycle regulation.

The role of the metabolic oscillator in cell-cycle control is supported by evolutionary findings. An amino acid sequence-based reconstruction of the maximum-likelihood phylogeny of cell-cycle-regulating kinases has shown that the CDKs emerged late in the evolution of eukaryotes (Krylov et al., 2003). The metabolic oscillator could constitute the previously conjectured ancestral non-CDK controller driving DNA replication and segregation (Murray, 2004). We envisage that during evolution, the CDK oscillator was grafted onto the metabolic oscillator to finely tune the coordination between biomass formation and segregation (Pines, 2011; Tyson and Novak, 2008), reduce noise in the duration of the cell-cycle phases (Di Talia et al., 2007), and robustly order the cell-cycle phases.

Through our work, we open an avenue for the investigation of cell-cycle control. Future research will need to unravel the nature of the metabolic oscillator, which we found to oscillate in all nutrient conditions. Such research efforts require the development of novel methods to dynamically assess the activity of metabolic pathways in single cells. Only when the nature of the metabolic oscillator is discovered will be possible to unravel the precise molecular functioning of the proposed system of coupled oscillators, incorporating the recently identified connections from the cyclin/CDK machinery toward metabolic enzymes (Ewald et al., 2016; Zhao et al., 2016), or in the opposite direction (Shi and Tu, 2013), and the cyclic expression of metabolic enzymes (Silverman et al., 2010; Wyart et al., 2010).

Once fully unraveled, the metabolic oscillator and its connections to the CDK machinery could serve as targets for the manipulation of cell fate (dormancy or proliferation) (Vander Heiden et al., 2009; Pearce et al., 2009; Wang and Green, 2012) or therapeutic targets against proliferative disorders (Galluzzi et al., 2013).

EXPERIMENTAL PROCEDURES

Strains

All strains (Table S1) were constructed on the background of the prototrophic YSBN6 (Kümmel et al., 2010) and its HIS$^-$ auxotrophic version (YSBN16). The construction of all stains is described in Supplemental Experimental Procedures. Primer sequences are included (Table S2).

Cultivation

Cells were grown in minimal medium (Verduyn et al., 1992) supplemented with the appropriate carbon source (glucose, galactose, or pyruvate). Exponentially growing cells were loaded in the microfluidic dissection platform as described previously (Huberts et al., 2013; Lee et al., 2012). A detailed description of the pre-culturing and culturing schemes is provided in Supplemental Experimental Procedures.

Microscopy

We used Nikon-Ti inverted microscopes with either an Andor 897 Ultra EX2 EM-CCD camera or 2× Andor LucaR EM-CCD cameras (dual camera system for FRET measurements), together with the CooLED pE2 excitation system. For NAD(P)H measurements, cells were excited at 365 nm (15% light-emitting diode [LED] intensity/200-ms exposure), using a 350/50-nm band-pass filter, a 409-nm beam-splitter, and a 435/40-nm emission filter. For GFP measurements, cells were excited at 470 nm (15%/200 ms) using a 470/40-nm band-pass filter, a 495-nm beam-splitter and a 525/50-nm emission filter. For RFP measurements, cells were excited at 565 nm (15%/200 ms for mRFP1, 50%/600 ms for mCherry) using a 560/40-nm band-pass filter, a 585-nm beam splitter, and a 630/75-nm emission filter. For FRET measurements, the donor (CFP) was excited at 440 nm (5%/50 ms) using a 438/24-nm band-pass filter. Donor emission was recorded using a 458-nm beam-splitter and a 483/32-nm emission filter. Acceptor (YFP) emission was recorded using a 535/30-nm emission filter. Only for FRET imaging, 2 × 2 pixel binning and 3× electron multiplying (EM)-gain (within the linear amplification range) were applied during image acquisition. In the differential interference contrast (DIC) channel, the light of a halogen lamp was passed through a 420-nm beam splitter to exclude UV radiation and minimize cell damage during long-term acquisition. For the FRET measurements, a 60× Nikon Plan-Apochromat objective was used. For the observation of chromosomal bridges (Figure 6I), a 100× Nikon Super Fluor-Apochromat was used. For the rest of the measurements, a 40× Nikon Super Fluor-Apochromat was used. Images were taken every 5 min for fast-growth conditions, 10 min during slow growth, or 20 min during growth on 0.01 g/L glucose. NIS elements software was used to control the microscope.

Image Analysis

The BudJ plug-in (Ferrezuelo et al., 2012) for ImageJ (Schneider et al., 2012) was used to segment, track single cells, and measure the NAD(P)H, Cln2-EGFP, mGFP-AID, Cdc14-mCherry-AID fluorescence. The Whi5-EGFP localization was manually determined for each single cell. The FRET donor and acceptor signals were manually determined separately in each fluorescent channel. For the determination of the cellular perimeter and Hta2-mRFP1 abundance before and after Cdc14-AID depletion, cells were manually segmented using the DIC channel (as in Figure 6H) and ImageJ (Schneider et al., 2012). A detailed description of image analysis, including background estimation and clustered fluorescence quantification, is provided in Supplemental Experimental Procedures.

Signal Analysis

All single-cell fluorescent signals (NAD(P)H, ATP-FRET, and Cln2-EGFP) presented in Figures 2B, 2C, 4A, S3C, S4D, and S5 were de-trended by dividing with a fitted smoothing spline in order to remove low-frequency variations. In Figures 1A, 1B, 2B, 2C, 4A, S3A, S3B, and S5, spline functions (fitted to the raw or de-trended NAD(P)H or ATP signals) were added only for the visualization of the metabolic dynamics and were not used in further analysis. In the Cdc14-depletion experiments, spline functions (parameter value 5e-4) were used to de-noise the perimeter and the NAD(P)H oscillations and estimate the rate of perimeter increase and the NAD(P)H rate in single cells (Figure S6). Smoothing splines were fitted using the MATLAB Curve Fitting Toolbox.

SUPPLEMENTAL INFORMATION

Supplemental Information includes Supplemental Experimental Procedures, six figures, two tables, and four movies and can be found with this article online at http://dx.doi.org/10.1016/j.molcel.2016.11.018.

AUTHOR CONTRIBUTIONS

A.P. designed the study, developed all reporters, performed all experiments, and analyzed all data. B.N. contributed to the development of the study and performed the autocorrelation function analyses. E.C.W. performed the hazard function and autocorrelation function analyses. M.H. conceived, designed, and supervised the study. A.P. and M.H. wrote the manuscript.

ACKNOWLEDGMENTS

The authors thank Jakub Leszek Radzikowski and the Molecular Systems Biology group for helpful discussion; Andrew Millar, Marcel van Vugt, Peter van Haastert, Maarten Linskens, and Bayu Jayawardhana for discussion and critical comments on the manuscript; and Martí Aldea for advice and support on image analysis (BudJ toolbox). Financial support was provided by the EU ITN project ISOLATE (grant agreement 289995).

Received: June 1, 2016
Revised: September 26, 2016
Accepted: November 9, 2016
Published: December 15, 2016

REFERENCES

Amaral, N., Vendrell, A., Funaya, C., Idrissi, F.-Z., Maier, M., Kumar, A., Neurohr, G., Colomina, N., Torres-Rosell, J., Geli, M.-I., and Mendoza, M. (2016). The Aurora-B-dependent NoCut checkpoint prevents damage of anaphase bridges after DNA replication stress. Nat. Cell Biol. *18*, 516–526.

Aon, M.A., Cortassa, S., Lemar, K.M., Hayes, A.J., and Lloyd, D. (2007). Single and cell population respiratory oscillations in yeast: a 2-photon scanning laser microscopy study. FEBS Lett. *581*, 8–14.

Banyai, G., Baïdi, F., Coudreuse, D., and Szilagyi, Z. (2016). Cdk1 activity acts as a quantitative platform for coordinating cell cycle progression with periodic transcription. Nat. Commun. *7*, 11161.

Bardwell, L. (2004). A walk-through of the yeast mating pheromone response pathway. Peptides *25*, 1465–1476.

Barik, D., Baumann, W.T., Paul, M.R., Novak, B., and Tyson, J.J. (2010). A model of yeast cell-cycle regulation based on multisite phosphorylation. Mol. Syst. Biol. *6*, 405.

Bloom, J., and Cross, F.R. (2007). Multiple levels of cyclin specificity in cell-cycle control. Nat. Rev. Mol. Cell Biol. *8*, 149–160.

Brunetti, A.J., Aydin, M., and Buchler, N.E. (2016). Cell cycle Start is coupled to entry into the yeast metabolic cycle across diverse strains and growth rates. Mol Biol Cell *27*, 64–74.

Buchakjian, M.R., and Kornbluth, S. (2010). The engine driving the ship: metabolic steering of cell proliferation and death. Nat. Rev. Mol. Cell Biol. *11*, 715–727.

Costanzo, M., Nishikawa, J.L., Tang, X., Millman, J.S., Schub, O., Breitkreuz, K., Dewar, D., Rupes, I., Andrews, B., and Tyers, M. (2004). CDK activity antagonizes Whi5, an inhibitor of G1/S transcription in yeast. Cell *117*, 899–913.

Coudreuse, D., and Nurse, P. (2010). Driving the cell cycle with a minimal CDK control network. Nature *468*, 1074–1079.

Cox, D.R. (1972). Regression models and life-tables. J. R. Stat. Soc. Series B Stat. Methodol. *34*, 187–220.

Cross, F., Roberts, J., and Weintraub, H. (1989). Simple and complex cell cycles. Annu. Rev. Cell Biol. *5*, 341–396.

Di Talia, S., Skotheim, J.M., Bean, J.M., Siggia, E.D., and Cross, F.R. (2007). The effects of molecular noise and size control on variability in the budding yeast cell cycle. Nature *448*, 947–951.

Ewald, J.C., Kuehne, A., Zamboni, N., and Skotheim, J.M. (2016). The yeast cyclin-dependent kinase routes carbon fluxes to fuel cell cycle progression. Mol. Cell *62*, 532–545.

Feillet, C., Krusche, P., Tamanini, F., Janssens, R.C., Downey, M.J., Martin, P., Teboul, M., Saito, S., Lévi, F.A., Bretschneider, T., et al. (2014). Phase locking and multiple oscillating attractors for the coupled mammalian clock and cell cycle. Proc. Natl. Acad. Sci. USA *111*, 9828–9833.

Ferrezuelo, F., Colomina, N., Palmisano, A., Garí, E., Gallego, C., Csikász-Nagy, A., and Aldea, M. (2012). The critical size is set at a single-cell level by growth rate to attain homeostasis and adaptation. Nat. Commun. *3*, 1012.

Futcher, B. (2006). Metabolic cycle, cell cycle, and the finishing kick to Start. Genome Biol. *7*, 107.

Galluzzi, L., Kepp, O., Vander Heiden, M.G., and Kroemer, G. (2013). Metabolic targets for cancer therapy. Nat. Rev. Drug Discov. *12*, 829–846.

Gustavsson, A.-K., van Niekerk, D.D., Adiels, C.B., du Preez, F.B., Goksör, M., and Snoep, J.L. (2012). Sustained glycolytic oscillations in individual isolated yeast cells. FEBS J. *279*, 2837–2847.

Haase, S.B., and Reed, S.I. (1999). Evidence that a free-running oscillator drives G1 events in the budding yeast cell cycle. Nature *401*, 394–397.

Hartwell, L.H., Culotti, J., Pringle, J.R., and Reid, B.J. (1974). Genetic control of the cell division cycle in yeast. Science *183*, 46–51.

Hillenbrand, P., Maier, K.C., Cramer, P., and Gerland, U. (2016). Inference of gene regulation functions from dynamic transcriptome data. eLife *5*, e12188.

Huberts, D.H.E.W., Sik Lee, S., Gonzáles, J., Janssens, G.E., Vizcarra, I.A., and Heinemann, M. (2013). Construction and use of a microfluidic dissection platform for long-term imaging of cellular processes in budding yeast. Nat. Protoc. *8*, 1019–1027.

Imamura, H., Nhat, K.P., Togawa, H., Saito, K., Iino, R., Kato-Yamada, Y., Nagai, T., and Noji, H. (2009). Visualization of ATP levels inside single living cells with fluorescence resonance energy transfer-based genetically encoded indicators. Proc. Natl. Acad. Sci. USA *106*, 15651–15656.

Jones, R.G., Plas, D.R., Kubek, S., Buzzai, M., Mu, J., Xu, Y., Birnbaum, M.J., and Thompson, C.B. (2005). AMP-activated protein kinase induces a p53-dependent metabolic checkpoint. Mol. Cell *18*, 283–293.

Klevecz, R.R. (1969). Temporal order in mammalian cells. I. The periodic synthesis of lactate dehydrogenase in the cell cycle. J. Cell Biol. *43*, 207–219.

Klevecz, R.R., and Ruddle, F.H. (1968). Cyclic changes in enzyme activity in synchronized mammalian cell cultures. Science *159*, 634–636.

Klevecz, R.R., Bolen, J., Forrest, G., and Murray, D.B. (2004). A genomewide oscillation in transcription gates DNA replication and cell cycle. Proc. Natl. Acad. Sci. USA *101*, 1200–1205.

Krylov, D.M., Nasmyth, K., and Koonin, E.V. (2003). Evolution of eukaryotic cell cycle regulation: stepwise addition of regulatory kinases and late advent of the CDKs. Curr. Biol. *13*, 173–177.

Kümmel, A., Ewald, J.C., Fendt, S.-M., Jol, S.J., Picotti, P., Aebersold, R., Sauer, U., Zamboni, N., and Heinemann, M. (2010). Differential glucose repression in common yeast strains in response to HXK2 deletion. FEMS Yeast Res. *10*, 322–332.

Laxman, S., Sutter, B.M., and Tu, B.P. (2010). Behavior of a metabolic cycling population at the single cell level as visualized by fluorescent gene expression reporters. PLoS ONE *5*, e12595.

Lee, I.H., and Finkel, T. (2013). Metabolic regulation of the cell cycle. Curr. Opin. Cell Biol. *25*, 724–729.

Lee, S.S., Avalos Vizcarra, I., Huberts, D.H.E.W., Lee, L.P., and Heinemann, M. (2012). Whole lifespan microscopic observation of budding yeast aging through a microfluidic dissection platform. Proc. Natl. Acad. Sci. USA *109*, 4916–4920.

Lee, Y., Dominy, J.E., Choi, Y.J., Jurczak, M., Tolliday, N., Camporez, J.P., Chim, H., Lim, J.-H., Ruan, H.-B., Yang, X., et al. (2014). Cyclin D1-Cdk4 controls glucose metabolism independently of cell cycle progression. Nature *510*, 547–551.

Lloyd, D., Edwards, S.W., and Fry, J.C. (1982). Temperature-compensated oscillations in respiration and cellular protein content in synchronous cultures of Acanthamoeba castellanii. Proc. Natl. Acad. Sci. USA *79*, 3785–3788.

Lloyd, D., Salgado, L.E.J., Turner, M.P., Suller, M.T.E., and Murray, D. (2002). Cycles of mitochondrial energization driven by the ultradian clock in a continuous culture of Saccharomyces cerevisiae. Microbiology *148*, 3715–3724.

Lu, Y., and Cross, F.R. (2010). Periodic cyclin-Cdk activity entrains an autonomous Cdc14 release oscillator. Cell *141*, 268–279.

Morawska, M., and Ulrich, H.D. (2013). An expanded tool kit for the auxin-inducible degron system in budding yeast. Yeast *30*, 341–351.

Mori, T., Binder, B., and Johnson, C.H. (1996). Circadian gating of cell division in cyanobacteria growing with average doubling times of less than 24 hours. Proc. Natl. Acad. Sci. USA *93*, 10183–10188.

Müller, D., Exler, S., Aguilera-Vázquez, L., Guerrero-Martín, E., and Reuss, M. (2003). Cyclic AMP mediates the cell cycle dynamics of energy metabolism in Saccharomyces cerevisiae. Yeast *20*, 351–367.

Murray, A.W. (2004). Recycling the cell cycle: cyclins revisited. Cell *116*, 221–234.

Murray, D.B., Roller, S., Kuriyama, H., and Lloyd, D. (2001). Clock control of ultradian respiratory oscillation found during yeast continuous culture. J. Bacteriol. *183*, 7253–7259.

Nishimura, K., Fukagawa, T., Takisawa, H., Kakimoto, T., and Kanemaki, M. (2009). An auxin-based degron system for the rapid depletion of proteins in nonplant cells. Nat. Methods *6*, 917–922.

Nolte, D.D. (2015). Introduction to Modern Dynamics: Chaos, Networks, Space and Time (Oxford University Press).

Novak, B., and Mitchison, J.M. (1987). Periodic cell cycle changes in the rate of CO2 production in the fission yeast Schizosaccharomyces pombe persist after a block to protein synthesis. J. Cell Sci. *87*, 323–325.

Novak, B., Halbauer, J., and Laszlo, E. (1988). The effect of CO2 on the timing of cell cycle events in fission yeast Schizosaccharomyces pombe. J. Cell Sci. *89*, 433–439.

Oikonomou, C., and Cross, F.R. (2010). Frequency control of cell cycle oscillators. Curr. Opin. Genet. Dev. *20*, 605–612.

Orlando, D.A., Lin, C.Y., Bernard, A., Wang, J.Y., Socolar, J.E.S., Iversen, E.S., Hartemink, A.J., and Haase, S.B. (2008). Global control of cell-cycle transcription by coupled CDK and network oscillators. Nature *453*, 944–947.

Pearce, E.L., Walsh, M.C., Cejas, P.J., Harms, G.M., Shen, H., Wang, L.-S., Jones, R.G., and Choi, Y. (2009). Enhancing CD8 T-cell memory by modulating fatty acid metabolism. Nature *460*, 103–107.

Pines, J. (2011). Cubism and the cell cycle: the many faces of the APC/C. Nat. Rev. Mol. Cell Biol. *12*, 427–438.

Rahi, S.J., Pecani, K., Ondracka, A., Oikonomou, C., and Cross, F.R. (2016). The CDK-APC/C oscillator predominantly entrains periodic cell-cycle transcription. Cell *165*, 475–487.

Rattray, A.M.J., and Müller, B. (2012). The control of histone gene expression. Biochem. Soc. Trans. *40*, 880–885.

Saqcena, M., Menon, D., Patel, D., Mukhopadhyay, S., Chow, V., and Foster, D.A. (2013). Amino acids and mTOR mediate distinct metabolic checkpoints in mammalian G1 cell cycle. PLoS ONE *8*, e74157.

Schneider, C.A., Rasband, W.S., and Eliceiri, K.W. (2012). NIH Image to ImageJ: 25 years of image analysis. Nat. Methods *9*, 671–675.

Sherr, C.J., and Roberts, J.M. (2004). Living with or without cyclins and cyclin-dependent kinases. Genes Dev. *18*, 2699–2711.

Shi, L., and Tu, B.P. (2013). Acetyl-CoA induces transcription of the key G1 cyclin CLN3 to promote entry into the cell division cycle in Saccharomyces cerevisiae. Proc. Natl. Acad. Sci. USA *110*, 7318–7323.

Silverman, S.J., Petti, A.A., Slavov, N., Parsons, L., Briehof, R., Thiberge, S.Y., Zenklusen, D., Gandhi, S.J., Larson, D.R., Singer, R.H., and Botstein, D. (2010). Metabolic cycling in single yeast cells from unsynchronized steady-state populations limited on glucose or phosphate. Proc. Natl. Acad. Sci. USA *107*, 6946–6951.

Slavov, N., Macinskas, J., Caudy, A., and Botstein, D. (2011). Metabolic cycling without cell division cycling in respiring yeast. Proc. Natl. Acad. Sci. USA *108*, 19090–19095.

Sohn, H.Y., Murray, D.B., and Kuriyama, H. (2000). Ultradian oscillation of Saccharomyces cerevisiae during aerobic continuous culture: hydrogen sulphide mediates population synchrony. Yeast *16*, 1185–1190.

Strogatz, S.H. (2001). Exploring complex networks. Nature *410*, 268–276.

Strogatz, S.H. (2014). Nonlinear Dynamics and Chaos (Westview Press).

Takubo, K., Nagamatsu, G., Kobayashi, C.I., Nakamura-Ishizu, A., Kobayashi, H., Ikeda, E., Goda, N., Rahimi, Y., Johnson, R.S., Soga, T., et al. (2013). Regulation of glycolysis by Pdk functions as a metabolic checkpoint for cell cycle quiescence in hematopoietic stem cells. Cell Stem Cell *12*, 49–61.

Tu, B.P., Kudlicki, A., Rowicka, M., and McKnight, S.L. (2005). Logic of the yeast metabolic cycle: temporal compartmentalization of cellular processes. Science *310*, 1152–1158.

Tu, B.P., Mohler, R.E., Liu, J.C., Dombek, K.M., Young, E.T., Synovec, R.E., and McKnight, S.L. (2007). Cyclic changes in metabolic state during the life of a yeast cell. Proc. Natl. Acad. Sci. USA *104*, 16886–16891.

Tudzarova, S., Colombo, S.L., Stoeber, K., Carcamo, S., Williams, G.H., and Moncada, S. (2011). Two ubiquitin ligases, APC/C-Cdh1 and SKP1-CUL1-F (SCF)-β-TrCP, sequentially regulate glycolysis during the cell cycle. Proc. Natl. Acad. Sci. USA *108*, 5278–5283.

Tyson, J.J., and Novak, B. (2008). Temporal organization of the cell cycle. Curr. Biol. *18*, R759–R768.

Vander Heiden, M.G., Cantley, L.C., and Thompson, C.B. (2009). Understanding the Warburg effect: the metabolic requirements of cell proliferation. Science *324*, 1029–1033.

Verduyn, C., Postma, E., Scheffers, W.A., and Van Dijken, J.P. (1992). Effect of benzoic acid on metabolic fluxes in yeasts: a continuous-culture study on the regulation of respiration and alcoholic fermentation. Yeast *8*, 501–517.

Wang, R., and Green, D.R. (2012). Metabolic checkpoints in activated T cells. Nat. Immunol. *13*, 907–915.

Wang, Z., Fan, M., Candas, D., Zhang, T.-Q., Qin, L., Eldridge, A., Wachsmann-Hogiu, S., Ahmed, K.M., Chromy, B.A., Nantajit, D., et al. (2014). Cyclin B1/Cdk1 coordinates mitochondrial respiration for cell-cycle G2/M progression. Dev. Cell *29*, 217–232.

Watts, G. (2001). Three cell cycle scientists win Nobel prize. BMJ *323*, 823.

Wyart, M., Botstein, D., and Wingreen, N.S. (2010). Evaluating gene expression dynamics using pairwise RNA FISH data. PLoS Comput. Biol. *6*, e1000979.

Xu, Z., and Tsurugi, K. (2006). A potential mechanism of energy-metabolism oscillation in an aerobic chemostat culture of the yeast Saccharomyces cerevisiae. FEBS J. *273*, 1696–1709.

Yalcin, A., Clem, B.F., Imbert-Fernandez, Y., Ozcan, S.C., Peker, S., O'Neal, J., Klarer, A.C., Clem, A.L., Telang, S., and Chesney, J. (2014). 6-Phosphofructo-2-kinase (PFKFB3) promotes cell cycle progression and suppresses apoptosis via Cdk1-mediated phosphorylation of p27. Cell Death Dis. *5*, e1337.

Zhao, G., Chen, Y., Carey, L., and Futcher, B. (2016). Cyclin-Dependent Kinase Co-Ordinates Carbohydrate Metabolism and Cell Cycle in S. cerevisiae. Mol. Cell *62*, 546–557.